### Relativistic shock breakout from a stellar wind

### Alon Granot, Ehud Nakar & Amir Levinson

The Raymond and Beverly Sackler School of Physics and Astronomy, Tel Aviv University, Tel Aviv 69978, Israel

18 August 2017

#### ABSTRACT

We construct an analytic model for the breakout of a relativistic radiation mediated shock from a stellar wind, and exploit it to calculate the observational diagnostics of the breakout signal. The model accounts for photon escape through the finite optical depth wind, and treats the fraction of downstream photons escaping to infinity as an adiabatic parameter that evolves in a quasi-steady manner. It is shown that the shock is mediated by radiation even when a large fraction of the downstream photons escape, owing to self-generation and adjustment of opacity through accelerated pair creation. Relativistic breakout occurs at radii at which the total optical depth of the wind ahead of the shock is  $\sim (m_e/m_p)\Gamma_{sh}$ , provided that the local shock Lorentz factor  $\Gamma_{sh}$  exceeds unity at this location. Otherwise the breakout occurs in the Newtonian regime. A relativistic breakout is expected in a highly energetic spherical explosion  $(10^{52} - 10^{53} \text{ erg})$  of a Wolf-Rayet star, or in cases where a smaller amount of energy  $(\sim 10^{51} \text{ erg})$  is deposited by a jet in the outer layers of the star. The properties of the emission observed in such explosions during the relativistic breakout are derived. We find that for typical parameters about 10<sup>48</sup> ergs are radiated in the form of MeV gamma-rays over a duration that can range from a fraction of a second to an hour. Such a signal may be detectable out to 10-100 Mpc by current gamma-ray satellites.

### 1 INTRODUCTION

The first light that signals the death of a massive star is emitted upon emergence of the shock wave generated by the explosion from the star. Prior to its breakout the shock propagates in the dense stellar envelope, and is mediated by the radiation trapped inside it. The observational signature of the breakout event depends on the shock velocity and the environmental conditions, thus, detection of the breakout signal and the subsequent emission can provide a wealth of information on the progenitor (e.g., mass, radius, mass loss prior to explosion, etc.) and on the explosion mechanism.

When the shock approaches the edge of the stellar envelope it starts accelerating, owing to the sharp density gradient there. Under certain conditions the shock may become mildly and even ultra-relativistic as it reaches the edge of the star. For a relatively energetic spherical explosion of  $\sim 10^{52}$ erg this happens in compact stars with  $R_* \lesssim R_{\odot}$ , while for larger energies, and/or strongly collimated explosions, relativistic shocks are generated also in more extended progenitors (Tan et al. 2001; Nakar & Sari 2012; Nakar 2015). If the circumstellar density is low enough the shock breaks out and undergoes a sudden transition into a collisionless shock at the stellar edge. However, if the progenitor is surrounded by a thick enough stellar wind the shock continues to be radiation mediated as it propagates down the wind. The shock physical width then increases during its propagation since the optical depth of the wind decreases, until it reaches the causality scale,  $R_{sh}/\Gamma_{sh}^2$ , where  $R_{sh}$  and  $\Gamma_{sh}$ are the shock radius and Lorentz factor, respectively. At this point photons start leaking from the shock to the observer and shock breakout begins. As shown below, in case of relativistic shocks this process may be gradual and can possibly continue over decades in radius. This gradual evolution of the shock during the breakout phase can significantly alter the breakout signal, and is of special interest since Wolf-Rayet stars, which are thought to be the progenitors of long GRBs, and are also compact enough to have relativistic shock breakout in extremely energetic SNe (such as SN 2002ap), are known to drive strong stellar winds.

The breakout of relativistic radiation mediated shocks (RRMS) has been studied recently by Nakar & Sari (2012), who employed the infinite planar shock solutions obtain by Budnik et al. (2010) to show that such episodes give rise to a flash of gamma-rays with very distinctive properties. However, their analysis is applicable to progenitors in which the breakout and the subsequent transition to a collisionless shock take place at the stellar edge, but not to the gradual breakouts anticipated in situations wherein the progenitor is surrounded by a thick stellar wind, as described above. Shock breakout from a stellar wind has been studied thus far only in the non-relativistic regime, where the shock structure and the physics underlying the breakout process are fundamentally different (e.g. Ofek et al. 2010; Balberg & Loeb 2011; Chevalier & Irwin 2011; Svirski & Nakar 2014a,b)

The purpose of this paper is to find the observational signature of the breakout of a RRMS from a stellar wind. The key to that is a proper modeling of the structure of RRMS as photon leakage starts. Here we do that using

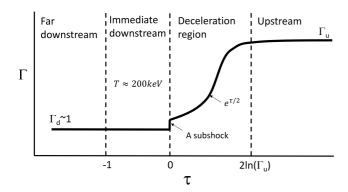


Figure 1. Schematic illustration of the Lorentz factor profile, as measured in the shock frame, of an infinite planar RRMS with a photon starved upstream, based on the results of Budnik et al. 2010. The properties of the different regions indicated in the figure are described in the text.

an analytic approach. To be concrete, we suppose that the shock evolves in an adiabatic manner, in the sense that at any given moment its structure can be described by a steady solution subject to the local wind conditions. Upon generalizing the infinite planar shock solutions of Budnik et al. (2010) to finite shocks with photon escape, we obtain a family of RRMS solutions which is characterized by one parameter - the fraction of downstream photons escaping the shock to infinity. Using these solutions we find the location in the stellar wind where its optical depth cannot support a RRMS anymore and the shock transforms into a collisionless shock.

Below, we first  $(\S 2)$  describe and extend the analytic solution of the structure of a RRMS propagating in a medium with and infinite optical depth which was derived by Nakar & Sari (2012) based on the numerical solutions of Budnik et al. (2010). We note that this solution is applicable only to a RRMS that propagates in a photon poor medium, as expected in stellar envelopes and winds. Under these conditions the photons that mediate the shock must be generated within the shock transition layer or in the immediate downstream (see Bromberg et al. 2011 for a discussion on the relative importance of photons created in the shock and photons advected by the upstream flow). We then (§3) generalize the analytic model to incorporate photon escape and apply it (§4) to find the criterion for shock breakout. In section §5 we employ these results to predict the observational signature of a relativistic breakout from a wind. We find a closure relation that the duration, temperature and energy of the breakout pulse must satisfy, and then proceed to calculate the observed emission expected in a stellar explosion, as a function of the explosion and progenitor parameters. We also discuss briefly the difference between a breakout from a stellar wind and a breakout from a stellar edge. We conclude in §6.

## 2 THE STRUCTURE OF AN INFINITE PLANAR RRMS

In this section we outline the analytic solution of a steady, infinite planar RRMS propagating in a photon starved medium. This solution was derived by Nakar & Sari (2012), based on the numerical solution obtained by Budnik et al.

(2010). The main assumption underlying these solutions is that all the plasma components (protons, electrons and pairs) are tightly coupled and behave as a single fluid. This assumption is well justified, since the interaction between the various plasma components occurs over scales of the order of the plasma skin depth, which is shorter than the shock width by many orders of magnitude.

Budnik et al. (2010) find that the shock structure can be divided to four regions which are shown schematically in figure 1. As seen in the shock frame these regions are:

- (i) The upstream unshocked cold plasma moving at Lorentz factor  $\Gamma_u = \Gamma_{sh} \gg 1$ . The energy density in this region is dominated by the rest mass of the baryons, and is given by  $\Gamma_u^2 n_u m_p c^2$ , where  $n_u$  is the proton proper density far upstream,  $m_p$  is the proton mass and c the speed of light.
- (ii) The deceleration region  $\Gamma$  is decreasing from  $\Gamma_u$  to the downstream value  $\Gamma_d \approx 1$ . The deceleration is driven by the interaction of counter-streaming photons (those moving from the downstream towards the upstream) with the plasma flowing towards the downstream, mostly through Compton scattering of electron-positron pairs, and pair loading via  $\gamma\gamma$  annihilation. Budnik et al. (2010) find that at the end of the deceleration zone there is a Newtonian collisionless subshock, which is unimportant for our modeling. (iii) The immediate downstream - the region just downstream of the shock from which the counter-streaming photons that decelerate the relativistic bulk plasma originate. Its optical depth is  $\tau \sim 1$ . The immediate downstream temperature is set by the rate of photon production, mostly through free-free emission, over the available time (roughly the advection time). It equals to  $\sim 200$  keV and is largely insensitive to the shock Lorentz factor. The reason is that in this regime the pair density and the resultant photon production rate increase exponentially with increasing temperature, thereby acting as a thermostat that keeps the immediate downstream temperature nearly constant over a large range of shock Lorentz factors. This regulation mechanism ceases to operate once the temperature exceeds the value above which the dependence of the pair production rate on temperature becomes linear rather than exponential. In this regime the analytic model derived below breaks down. How high the shock Lorentz factor should be for this to occur is unclear at present. The analysis of Budnik et al. (2010) indicates that the model is valid at least up to  $\Gamma_{sh} = 30$ . (iv) The far downstream - where the radiation ultimately approches full thermodynamic equilibrium, and the radiation energy density satisfies  $e_r = a_{BB}T_d^4$ , where  $T_d$  is the far downstream temperature which for relativistic shocks is vastly smaller than the immediate downstream temperature. The photons from this region cannot stream back to the de-

The analytic model computes the structure of the deceleration region where the flow is still relativistic in the shock frame ( $\Gamma \gtrsim 2$ ). In this region the two-stream approximation can be used. One stream (the primary beam) consists of the lasma constituents (protons, electrons and pairs) and the back-scattered photons, all of which move towards the downstream. The counterstream contains photons, each having an energy of  $\sim m_e c^2$  in the shock frame, that were generated in the immediate downstream and move towards the upstream.

celeration region and it is, therefore, unimportant for our

Since every counterstreaming photon that interacts with the primary beam is converted either to a backscattered photon or a lepton, it is convenient to treat the pairs created inside the shock and the backscattered photons as a single species. The proper density of this species is the sum  $n_l = n_{\gamma, \to d} + n_{\pm}$ , where  $n_{\gamma, \to d}$  and  $n_{\pm}$  denote the proper densities of backscattered photons and pairs, respectively. We use this spices also to define the loading parameter  $x_l \equiv \frac{n_l}{n_l}$  where  $n \equiv n_p = n_e$  is the proper baryon density which must be equal to the density of electrons advected from the far upstream (i.e., not created inside the shock) by virtue of charge conservation. The shock equations, derived in the appendix, subject to the boundary condition  $x_l = 0$ far upstream where counterstreaming photons do not reach, then reduce to the following conservation laws: baryon number conservation,

$$n_u \Gamma_u \beta_u = n \Gamma \beta, \tag{1}$$

and energy conservation (see equation A11),

$$\Gamma_u = \Gamma(1 + 4(x_l + 1)\hat{T}\mu),\tag{2}$$

where  $\mu = \frac{m_e}{m_p}$ ,  $\hat{T} = kT/m_ec^2$  is the dimensionless temperature,  $\beta$  is the plasma 3-velocity with respect to the shock frame and  $\Gamma$  the corresponding Lorentz factor. Henceforth, the subscript 'u' refers to quantities at the far upstream. The energy equation, Eq.(2), neglects the contribution of the counterstreaming photons to the total energy flux, which is justified in the region where the primary beam is sufficiently relativistic.

The conservation of photon-and-pair fluxes implies  $d(\Gamma n_l) = -n'_{\gamma, \to u} d\tau$ , where  $n'_{\gamma, \to u} = \Gamma n_{\gamma, \to u}$  is the density of counterstreaming photons, as measured in the shock frame, and  $\tau$  is the net optical depth for conversion of counterstreaming photons including Compton scattering and pair creation, defined explicitly in equation A7. Now, in an infinite shock counterstreaming photons cannot escape the system. Consequently, at any given location within the shock, for each counterstreaming photon there corresponds a quanta of the  $n_l$  species moving towards the downstream, that is,  $n'_{\gamma, \to u} = \Gamma n_l$ . In terms of  $x_l = n_l/n$  we then obtain:

$$\frac{dx_l}{d\tau} = -x_l. (3)$$

To find the temperature inside the shock we note that every collision of a counterstreaming photon with the primary beam adds additional quanta of proper energy  $\eta \Gamma m_e c^2$  to the primary beam, where  $\eta$  is a factor of order unity that depends on the exact energy and angular distributions of pairs and photons inside the shock, as well as other details ignored in the analytic model. Given that this added energy is shared among the entire plasma constituents, the plasma temperature can be approximated as:

$$\hat{T} = \frac{\eta \Gamma n_l}{n_l + n_e + n_p} = \eta \frac{\Gamma x_l}{x_l + 2}.$$
(4)

Equations 1-4 are applicable in the entire region where  $\Gamma \gtrsim 2$ , including the far upstream<sup>1</sup>. Thus, their solution pro-

vides the structure of the upstream and deceleration zone up to the point that the plasma flow becomes mildly relativistic. This set of equations can be solved analytically. From equation 1 and 2 we obtain

$$\Gamma(x_l) = \frac{\sqrt{1 + 16\mu\Gamma_u\eta\frac{x_l(x_l+1)}{x_l+2}} - 1}{8\mu\eta\frac{x_l(x_l+1)}{x_l+2}}$$

$$\approx \begin{cases} \Gamma_u & x_l \ll \frac{1}{16\mu\Gamma_u\eta} \\ \sqrt{\frac{\Gamma_u}{4x_l\mu\eta}} & x_l \gg \frac{1}{16\mu\Gamma_u\eta} \end{cases}$$
(5)

The value of  $x_l$  that separates the two regimes marks the transition between the deceleration zone and the upstream. Extending the solution to the immediate downstream where  $\Gamma \approx 1$  we obtain, using equation 2, an approximation for the value of  $x_l$  in the immediate downstream:  $x_0 \approx \frac{\Gamma_u}{4\mu\eta}$ . This ignores the energy of counterstreaming photons that may not be negligible there. However, it is not expected to alter this result by more than a factor of 2. Choosing  $\tau = 0$  at the subshock, which marks the transition between the immediate downstream and the deceleration zone, equation 3 yields

$$x_l = \frac{\Gamma_u}{4\mu\eta} e^{-\tau}. (6)$$

Equations 5 and 6 implies that in the shock transition layer

$$\Gamma(\tau) \approx e^{\tau/2}, \qquad (\Gamma < \Gamma_u).$$
 (7)

These equations reveal the unique nature of RRMS in a photon poor medium. The shock generates its own opacity via rapid pair production. It is doing so exponentially in the deceleration region within an optical depth of a few from the immediate downstream. The width of the shock, measured in terms of the net optical depth of a counterstreaming photon, is  $\Delta \tau \approx 2 ln(\Gamma_u)$ .

To verify the validity and check the accuracy of our model we compare it to the numerical solution derived by Budnik et al. (2010). They present their results using the Thomson optical depth of the shock (including the pairs created within the shock),  $\tau_*$ . Now, the cross-sections for Compton scattering and pair production of a photon heading towards the upstream are both in the KN regime, and are approximately equal (to better than a factor of 2). Thus, we can write  $d\tau_* = \frac{\sigma_T}{\sigma_{KN}} d\tau$ , where  $\sigma_T$  is the Thomson cross-section and

$$\sigma_{KN} \approx \frac{3}{8} \cdot \frac{\ln(2\Gamma(1+a\hat{T}))}{\Gamma(1+a\hat{T})} \sigma_T.$$
 (8)

Here we use the fact that the energy of counterstreaming photons is  $\sim m_e c^2$  with respect to the shock frame, and that  $\Gamma(1+a\hat{T})\gg 1$ . The factor 'a' accounts for the exact angular distributions of the colliding streams, and is typically of order unity.

Figure 2-4 show a comparison of  $\Gamma$ ,  $\hat{T}$  and  $x_l$  profiles as a function  $\tau_*/\Gamma_u$  obtained using our analytic model and the numerical model of Budnik et al. (2010) (their figures 6, 8 & 10). The free parameters in this fit are  $\eta$  and a which are expected to be of order unity. We obtain good fits for  $\eta=0.45-0.55$  and a=1.5-2.5. The agreement is not exact but it is remarkable given the simplicity of the analytic model. In particular, the agreement between the Lorentz factor profiles

<sup>&</sup>lt;sup>1</sup> Here we account for the electrons that are advected to the shock with the protons from the far upstream, which were neglected by Nakar & Sari (2012). We therefore extend their solution, which was applicable only to the deceleration region ,also to the upstream where advected electrons dominate over created pairs.

### 4 Granot, Nakar & Levinson

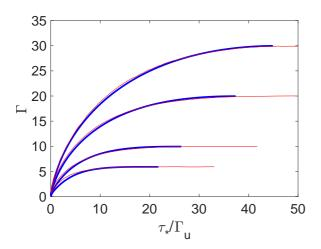
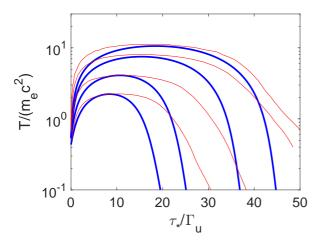


Figure 2. A comparison of the Lorentz factor profiles obtained by Budnik et al. 2010 (thin red lines) and our analytic solution (thick blue lines), for shocks with  $\Gamma_u$  =6, 10, 20, 30. Here  $\tau_*$  is the (pairs loaded) Thomson optical depth. The values of  $\eta$  and a are chosen in order to obtain the best fit for each  $\Gamma_u$  profile, and are all in the range  $\eta = 0.45 - 0.55$  and a = 1.5 - 2.5.



**Figure 3.** Temperature profiles. Notations are the same as in figure 2.

and, hence, the shock width is very good. The temperature and pair loading predicted by the analytic model also show general agreement, although there is a significant deviation, especially in the far upstream where our model predicts that pair loading and heating start closer to the shock and grow faster. This is most likely due to our choice of constant values for  $\eta$  and a across the entire shock, which corresponds to a constant angular distribution and a constant energy of the counterstreaming photons. However, in reality only the most energetic photons survive in the far upstream due to their smaller cross-section, and this should render  $\eta$  and a dependent on optical depth.

Finally in order to determine the location at which photons start escaping from a shock propagating in a medium having a finite optical depth, we need to find the width of the shock in terms of the pair unloaded Thomson optical

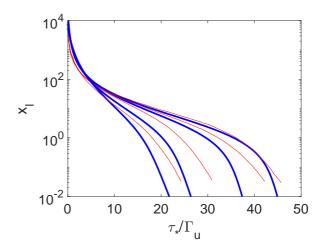


Figure 4. Profiles of the loading parameter. The profiles of Budnik et al. 2010 (their figure 10), which are given in terms of positron loading are multiplied by 3, assuming a comparable number of positrons and backscattered photons. Notations are the same as in figure 2.

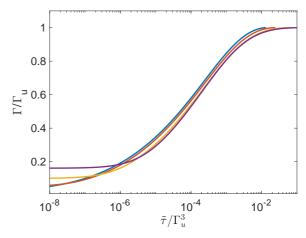


Figure 5. Profiles of the Lorentz factor (normalized to  $\Gamma_u$ ) as a function of  $\tilde{\tau}/\Gamma_u^3$ , for shocks with  $\Gamma_u=6$ , 10, 20, 30. Here  $\tilde{\tau}$  is the pairs unloaded Thomson optical depth. The values of  $\eta$  and a are the same as those used in figure 2. This figure demonstares that all the shocks have similar shapes as a function of  $\tilde{\tau}/\Gamma_u^3$  and that their width is consistent with the estimate given in equation 10.

depth,  $\tilde{\tau}$ :

$$d\tilde{\tau} = \frac{d\tau_*}{x_l + 1} = \frac{\sigma_T}{\sigma_{KN}(x_l + 1)} d\tau. \tag{9}$$

Note that in a medium with a given density  $n, d\tilde{\tau}$  is translated directly to a physical distance,  $dz = d\tilde{\tau}/(n\sigma_T)$ . Photon escape will commence once the optical depth to infinity approaches the optical depth of the shock transition layer. In this region  $x_l \propto \Gamma^{-2}, x_l \gg 1$  and  $\hat{T} \approx \Gamma$ , therefore  $d\tilde{\tau} \propto \Gamma^4 d\tau$ . Since in the deceleration zone  $\Gamma \propto e^{\tau/2}$ , most of the shock width is contained near the transition from the deceleration region to the upstream, where  $\tau$  varies by about one and  $\Gamma$  drops from  $\Gamma_u$  by about one e-folding. In this region  $x \approx \frac{1}{16\mu\Gamma_u\eta}$  (see equation 5) and  $\Gamma \approx \Gamma_u$ . Therefore, from equation 9 we find that the shock width, measured in

terms of the pair-unloaded Thomson optical depth, is

$$\Delta \tilde{\tau} \approx 10 \eta \mu \Gamma_u^3 \approx \frac{\Gamma_u^3}{400}.$$
 (10)

Figure 5 exhibits the Lorentz factor profile of the shock as a function of  $\tilde{\tau}/\Gamma_u^3$  for several values of  $\Gamma_u$ . It indicates that the profile is universal when plotted as a function of  $\tilde{\tau}/\Gamma_u^3$ , and that the shock width is consistent with equation 10 in all cases. We emphasize that this is the main and most important result of our analysis in this section.

It is interesting to compare the optical depth needed by the upstream to sustain the shock in the Newtonian and relativistic regimes, and its evolution with the shock 4-velocity,  $\Gamma_{sh}\beta_{sh}$ . In the Newtonian regime no pairs are created and there are no relativistic photons or electrons so the relevant cross-section is the Thomson cross-section. Thus,  $\tilde{\tau} = \tau$  and  $\Delta \tilde{\tau} \approx 1/\beta_{sh}$ . In this regime the shock width is determined by the requirement that the velocity at which photons from the downstream diffuse towards the upstream is comparable to the shock velocity and thus the shock becomes narrower with increasing velocity. In the relativistic regime, on the other hand, there is no diffusion and the width of the shock is dominated by pair production and Klein-Nishina effects. Thus, although  $\Delta \tau$  depends only logarithmically on  $\Gamma_{sh}$ ,  $\Delta \tilde{\tau}$ (and thus the shock physical width) depends sensitively on the shock Lorentz factor (as  $\Gamma_{sh}^3$ ). The reason is that increasing the shock Lorentz factor reduces both the cross-section and the number of pairs that are produced at the location where the shock starts decelerating. Note, however, that the transition in the physical shock width between the Newtonian and the relativistic regimes is not continuous. The width of a relativistic shock with a moderate Lorentz factor is  $\Delta \tilde{\tau} \ll 1$ , much narrower than the fastest Newtonian shock. This stems from the vigorous pair production that ensues once the shock velocity approches the speed of light. Consequently, the shock is narrowest when  $\Gamma_{sh}\beta_{sh}\approx 1$ , for which  $\Delta \tilde{\tau} \sim \mu$ , although our solution is not applicable in this regime.

# 3 THE STRUCTURE OF RRMS WITH PHOTON ESCAPE

Next we explore how the structure of a RRMS changes as photons starts escaping from the downstream to infinity, owing to a finite upstream optical depth. The generalized model uses the same assumptions invoked in the above treatment of infinite shocks, namely a steady structure in the shock frame, and immediate downstream temperature of  $\sim 200$ keV. We discuss the validity of these two assumptions in the next section, after presenting the solution. We also assume that the net energy carried by the escaping photons is subdominant. Under these assumptions equations 1, 2 and 4 remain unchanged. The only difference appears when deriving equation 3 since not all the counterstreaming photons return to the downstream. At any location inside the shock transition layer there is a constant number density of photons (when measured in the shock frame), denoted by  $n'_{esc}$ , that head towards the upstream without ever returning (see appendix for details). Thus,  $\Gamma n_l = n'_{\gamma, \to u} - n'_{esc}$  and equa-

$$\frac{dx_l}{d\tau} = -x_l - x_{esc} = -x_l - f\frac{\Gamma_u}{4\eta\mu},\tag{11}$$

where  $x_{esc} = \frac{n'_{esc}}{\Gamma n}$  and we define  $f \equiv \frac{x_{esc}}{x_0} \approx x_{esc} \frac{4\eta\mu}{\Gamma_u}$  to be the fraction of downstream photons that escape to infinity, with 0 < f < 1, whereby f = 0 corresponds to the limt of no escape (solved in the previous section) and  $f \simeq 1$  to a full shock breakout.

Before proceeding to discuss the general solution, it is instructive to examine the behaviour of the solution near the edge of a finite shock of total optical depth to infinity  $\tau_{\infty}$ , and compare it to the properties of a shock with an infinite optical depth at the location  $\tau = \tau_{\infty}$  (in both  $\tau$ is measured from the subshock towards the upstream). In both shocks the number of photons that flow towards the upstream is the same,  $n'_{\gamma,\to u}(\tau_\infty) = n_0 e^{-\tau_\infty}$ . In the finite shock  $n'_{\gamma,\to u}(\tau_\infty) = n'_{esc}$  while in the infinite shock  $n'_{\gamma,\to u} =$  $n_l$ . Now, in the finite shock there are no pairs or photons coming with the plasma at  $\tau_{\infty}$ , namely  $x_l(\tau_{\infty}) = 0$ , while in the infinite shock  $x_l(\tau_{\infty}) = x_{esc}$ . Following the growth of  $x_l$ in the finite shock from the edge towards the downstream we see that as long as  $x_l < x_{esc}$  equation 11 dictates  $x_l(\tau) \simeq$  $x_{esc}(\tau_{\infty}-\tau)$ . Thus, within an optical depth of about unity the number of returning pairs and photons in the finite shock becomes comparable to that of the infinite shock regardless of the value of f. This is naively expected since, on the average, over this depth every photon that flow towards the upstream is scattered or create a pair. This implies that since the optical depth of an infinite shock is larger than unity  $(\approx 2 \ln \Gamma_{sh})$ , when the optical depth is finite and photons escape, the shock can compensate for that loss by producing enough returning particles faster than in an infinite shock, as long as  $\tau_{\infty} \gtrsim 1$ . Below we solve the full equations and show that this is indeed the case.

Since equations 1 and 2 are valid also when photons escape so does equation 5 for  $\Gamma(x_l)$ . Combined with equation 11, in the region where  $x_l > 1$  we obtain  $d\tau \approx \frac{2\Gamma_u - \Gamma}{\Gamma[\Gamma_u(1+f\Gamma^2) - \Gamma]}d\Gamma$ , which can be integrated analytically to yield the shock profile. This expression shows that photon escape becomes important when  $f > 1/\Gamma_u^2$ . For lower values of f the shock is basically similar to an infinite shock, while for larger values we can approximate

$$d\tilde{\tau} \approx \frac{\mu \Gamma_u}{f} \left[ \frac{8a}{3\eta} \frac{G(2-G)}{(1-G)\ln(2a\Gamma_u^2 G)} \right] dG, \tag{12}$$

where  $G \equiv \Gamma/\Gamma_u$ . We used the approximated temperature  $\hat{T} \approx \eta \Gamma$  which is applicable for  $x_l > 1$  and the relation  $x+1 = \frac{\Gamma_u - \Gamma}{4\eta\mu\Gamma^2}$  which stems from equations 2. To find the width of the shock,  $\Delta \tilde{\tau}$ , when photon escape is important we integrate equation 12 from  $G = 1/\Gamma_u$  to G = 0.9, which we arbitrarily chose as the boundary between the deceleration zone and the upstream. We find that the integral over the term in the parenthesis depends weakly on  $\Gamma_u$  and is of order unity and therefore  $\Delta \tilde{\tau} \approx \frac{\mu \Gamma_u}{f}$ . Changing the upper limit of the integration to G = 0.99 changes the result by about a factor of 2. Therefore the shock width in terms of the pair unloaded Thomson optical depth is

$$\Delta \tilde{\tau} = \begin{cases} 10\eta \mu \Gamma_u^3 & f \ll \frac{1}{\Gamma_u^2} \\ \frac{\mu \Gamma_u}{f} & f \gg \frac{1}{\Gamma_u^2} \end{cases}$$
 (13)

Figure 6 shows  $\Delta \tilde{\tau}$ , obtained from integration of the full equations (without assuming  $x_l > 1$ ), as a function  $\mu \Gamma_u / f$  for several values of  $\Gamma_u$  (i.e., on each curve  $\Gamma_u$  remains constant while f varies). It shows that equation 13 provides an

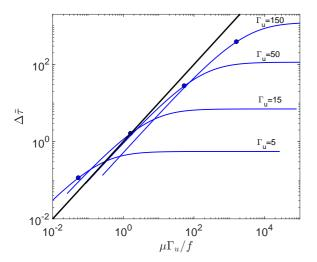


Figure 6. The shock width  $\Delta \tilde{\tau}$  as a function of  $\mu \Gamma_u/f$ . On each of the four curves f varies while  $\Gamma_u=5$ , 15, 50 & 150 remains constant.  $\Delta \tilde{\tau}$  is measured using the full analytic solution with  $\eta=0.5$  and a=2, and is defined as the pair unloaded Thompson optical depth where  $\Gamma=0.9\Gamma_u$ . The circles mark the location where  $f=1/\Gamma_u^2$ , at which equation 13 predicts a transition in the shock width dependence on f. The solid black line is a plot of  $\Delta \tilde{\tau}=\mu \Gamma_u/f$ , and is given for guidance. This figure indicates that the width is given by equation 13 to within an order of magnitude.

order of magnitude estimate of the shock width as a function of the photon escape fraction. Figure 7 shows the Lorentz factor profile as a function of  $\tilde{\tau}$ . It shows how the shock becomes narrower when the fraction of escaping photons increases. Once the optical depth to infinity becomes too small and photon escape starts affecting the shock structure, the shock adjusts itself and becomes narrower to match the finite optical depth. This is in contrast to a Newtonian shock which cannot adjust itself, and therefore full shock breakout follows within a dynamical time after photon escape starts becoming non-negligible. Figures 8-9 show the mechanism that allows the shock to adjust its width - a rapid buildup of  $x_l$  within a unit interval of the optical depth  $\tau$ , which compensates for the lack of backscattered photons at  $\tau > \tau_{\infty}$ . As can be seen from figures 7-9, the structures of all shocks with different values of f converge while the flow is still relativistic, before it approaches the downstream ( $\tau \leq 1$ ), even when photon escape strongly affects the shock width. This result supports our assumption that the conditions in the immediate downstream are similar in all shocks, even in the presence of a significant photon escape.

### 4 SHOCK BREAKOUT

In the previous section we derived the steady state structure of a RRMS with photon escape. In astrophysical settings the shock propagates in a medium having a finite Thomson depth to infinity  $\tilde{\tau}_{\infty}$ . Note that we use  $\tilde{\tau}$  to describe the optical depth of the circumstellar medium since no pairs are created before it is encountered by the shock. For typical settings we expect both  $\Gamma_{sh} = \Gamma_u$  and  $\tilde{\tau}_{\infty}$  to vary with time. Then, once  $\tilde{\tau}_{\infty} \approx \Delta \tilde{\tau}(f=0)$  photons starts leaking out. However, since the shock width continuously adjusts,

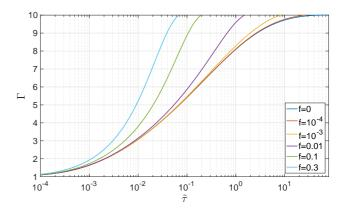


Figure 7. Lorentz factor profiles as a function of  $\tilde{\tau}$  for shocks with  $\Gamma_u=10$  and different f values.

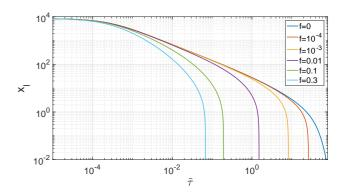


Figure 8. Profiles of the loading parameter as a function of  $\tilde{\tau}$  for shocks with  $\Gamma_u=10$  and different f values.

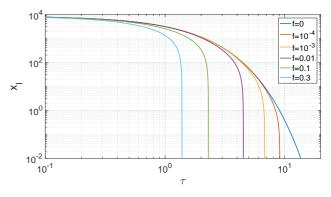


Figure 9. Profiles of the loading parameter as a function of  $\tau$  for shocks with  $\Gamma_u = 10$  and different f values.

the breakout is gradual and the fraction of shock energy that escapes at every location can be estimated roughly from the relation  $\tilde{\tau}_{\infty} \approx \Delta \tilde{\tau}(f)$ , that yields  $f \approx \frac{\mu \Gamma_u}{\tilde{\tau}_{\infty}}$ . A full breakout will take place once  $f \sim 1$ , whereby  $\tilde{\tau}_{bo} \sim \mu \Gamma_u$ .

Two basic assumptions underlying the solution derived in the previous section; the first one is that the system is locally in a steady state, and the second one is that the immediate downstream temperature is maintained at  $\sim m_e c^2/3$  throughout the evolution. The former assumption is marginally justified during a breakout from a wind, since all the shock properties (e.g., f and  $\Gamma_{sh}$ ) vary on the same timescale as it takes a photon from the immediate down-

stream to cross the shock and reach the upstream. Thus, our solution is a crude approximation, yet we expect our estimate of f not to be strongly affected by the temporal evolution of the shock structure, as it merely depends on the optical depth ahead of the shock; namely, f can be treated as an adiabatic parameter. The latter assumption, that the immediate downstream temperature is maintained at  $\sim m_e c^2/3$ , holds provided our solution for the shock structure is stable. We have shown that a self-consistent solution of the shock structure exists under this assumption, but whether it is stable is yet an open issue. Thus, although our results are self-consistent and based on educated assumptions they still need to be confirmed by a full time-dependent analysis of the breakout process.

The optical depth to infinity at the time of full breakout,  $\tilde{\tau}_{bo}$ , can be estimated using another method, which is independent of the shock structure, except for the assumption that the temperature in the immediate downstream is  $\sim m_e c^2/3$ . As seen in the upstream frame, on full breakout the shock releases from the immediate downstream an energy that is comparable to the energy that is in the shock transition layer, namely  $E_{bo} \approx \Gamma_u^2 M_{bo} c^2$  where  $M_{bo}$  is the mass in the transition layer, which is approximately the mass contained between the immediate downstream and infinity. If the energy is released in the form of  $\sim \Gamma_u m_e c^2$  photons (in the upstream rest frame) then the total number of photons upon breakout is  $N_{\gamma,bo} \approx E_{bo}/\Gamma_u m_e c^2 \approx \Gamma_u M_{bo}/m_e$ . Now, for photons to be able to escape to infinity their interaction with the upstream electrons should not lead to a runaway of pair production. Namely, the number of pairs created by this interaction must be lower than the number of electrons in the upstream. The breakout will take place once these numbers are comparable, namely  $N_{\gamma,bo}\tau_{\gamma\gamma} \approx N_e \approx M_{bo}/m_p$ . The energy of photons escaping to infinity is  $\sim \Gamma_u m_e c^2$  and they produce pairs on photons that were scattered once on electrons in the upstream and therefore their energy is also  $\sim \Gamma_u m_e c^2$ , therefore  $\tau_{\gamma\gamma} \sim \tilde{\tau}_{\infty} \sigma_{KN} / \sigma_T \sim \tilde{\tau}_{\infty} / \Gamma_u^2$ . We therefore obtain that the breakout takes place once  $\tilde{\tau}_{\infty}$  satisfies,

$$\tilde{\tau}_{bo} \approx \mu \Gamma_u,$$
 (14)

in agreement with criterion derived above by setting f=1 in equation 13.

Equation 14 is the criterion for breakout provided the shock is relativistic i.e,  $\Gamma_{sh} > 1$ . However if the shock decelerates to mildly relativistic velocities before this condition is satisfied then the temperature behind the shock drops to  $\sim 50-100$  keV, and the pair production rate is strongly suppressed. As a result the shock cannot generate its own opacity any longer and if  $\tilde{\tau}_{\infty} < 1$  it breaks out. Consequently, in order to determine the breakout properties in a given astrophysical setting we need to examine the overall shock evolution and see whether equation 14 is satisfied (i.e.  $f \approx 1$ ) before or after the shock becomes Newtonian. If it is satisfied before then the breakout is relativistic, and takes place once  $\tilde{\tau}_{bo} \approx \mu \Gamma_u$ . If not, then the breakout occurs when  $\Gamma_{sh} \approx 1$ , given that at this time  $\tilde{\tau} < 1$ .

#### 5 OBSERVATIONAL IMPLICATIONS

In the preceding sections we computed the dependence of the fraction of photons escaping from a RRMS on the optical depth to the observer. Here we consider the observational signature of this process. We first find a closure relation that must be satisfied by the relativistic breakout observables, and then calculate the signature of a RRMS breakout through a stellar wind.

### 5.1 Observables as functions of $R_{bo}$ and $\Gamma_{bo}$ and a closure relation

The three main observables of a complete RRMS breakout (i.e., f = 1), the duration,  $t_{bo}$ , the observed temperature  $T_{obs,bo}$  and the total emitted energy,  $E_{bo}$ , are determined by only two physical parameters, the breakout Lorentz factor  $\Gamma_{bo}$  and the breakout radius  $R_{bo}$ :

$$t_{bo} \approx \frac{R_{bo}}{2c\Gamma_{bo}^2} \approx 2R_{13}\Gamma_{10}^{-2} \text{ s},$$
 (15)

where  $R_{bo} = 10^{13} R_{13}$  cm and  $\Gamma_{bo} = 10 \Gamma_{10}$ ,

$$T_{obs,bo} \approx 200\Gamma_{bo} \text{ keV} = 2\Gamma_{10} \text{ MeV},$$
 (16)

and

$$E_{bo} = 3 \times 10^{48} \kappa_{0.2}^{-1} R_{13}^2 \Gamma_{10}^3 \text{ erg}, \tag{17}$$

where  $\kappa_{0.2}$  is the Thomson opacity per unit of mass in units of  $0.2~{\rm cm^2/gr}$ . In the last equation we used the optical depth of the shock at the time of breakout (equation 14) and  $E_{bo} \approx \Gamma_{bo}^2 M_{bo} c^2$  where  $M_{bo} \approx 4\pi R_{bo}^2 \tilde{\tau}_{bo}/\kappa$  is the mass in the shock layer upon breakout. Since these three observables depend on two breakout parameters they should satisfy a closure relation:

$$E_{bo} \approx 10^{48} \kappa_{0.2}^{-1} \left(\frac{t_{bo}}{1 \text{ s}}\right)^2 \left(\frac{T_{obs,bo}}{2 \text{ MeV}}\right)^7 \text{ erg.}$$
 (18)

Note the strong dependence on the observed temperature. Since the expected spectrum is not a blackbody this quantity is not accurately defined. This freedom allows for a wide range of breakout observables to be largely consistent with the closure relation. However, it does give some constraint on whether a given observation may be a result of a RRMS breakout. Note also that the above relations assume spherical symmetry. However since the breakout is relativistic it is enough if it is quasi-spherically symmetric over an opening angle that is larger than  $1/\Gamma_{bo}$ , as long as the observer line-of-sight falls within this opening angle.

#### 5.2 A RRMS breakout from a stellar wind

### 5.2.1 Spherical explosion

We consider a spherically symmetric explosion of a star in which the shock accelerates to relativistic velocities at the edge of the envelope, upon transitioning into a wind with an optical depth large enough to sustain it in a state of RRMS. As we will show this scenario is expected in sufficiently energetic explosions of Wolf-Rayet (WR) stars. We will also show (in the next subsection) that the following results may also be applicable, with some adjustments, to aspherical explosions.

The physical setting that we consider is as follows. The

explosion energy (kinetic energy at infinity) is E, the progenitor radius  $R_*$  and the ejecta mass  $M_{ej}$ . We approximate the density at the stellar edge as  $\rho_*(r) \propto (R_* - r)^3$ , where r is the radius, as expected for a WR star. The wind profile is  $\rho_w = Ar^{-2}$ , where A is a constant. To find the observed signature of a breakout from a wind in such settings we find first the Lorentz factor of the shock as it propagates through the wind, as function of the wind density and radius, and then apply equation 13 to find the emission that escapes to the observer.

Under the conditions considered here, the shock that was driven by the explosion at the center of the progenitor accelerates as it encounters the sharp density gradient near the stellar edge. For the density profile we use, once the shock becomes relativistic the acceleration follows the solution of Johnson & McKee (1971) (see also Tan et al. 2001 and Pan & Sari 2006). After shock crossing a rarefaction wave crosses the shocked stellar material, accelerating it farther. The final profile of the expanding stellar material after its acceleration ends satisfies  $E_*(\gamma) \propto m_*(\gamma) \gamma \propto \gamma^{-1.1}$ where  $E_*(\gamma)$  is the energy carried by stellar material with Lorentz factor  $> \gamma$  and  $m_*$  is the corresponding mass (Tan et al. 2001; Barniol Duran et al. 2015). It is convenient to find the normalization of  $E_*(\gamma)$  using the Lorentz factor of  $m_*$  that have an optical depth  $\tau = 1$  before the explosion, namely,  $m_{*,1} = 4\pi R_*^2/\kappa$ . Nakar & Sari (2012) find that<sup>2</sup>

$$\gamma_{*,1} \approx 50E_{53}^{1.7} M_{ej,5}^{-1.2} R_{*,11}^{-0.95},$$
(19)

where  $E=10^{53}E_{53}$  erg,  $M_{ej}=5M_{ej,5}~{\rm M}_{\odot}$  and  $R_*=10^{11}R_{*,11}~{\rm cm}.$ 

After the shock crosses the star it emerges into the wind and starts decelerating. In the process, in addition to the forward shock driven into the wind there is aslo a reverse shock driven into the expanding stellar material. The energy flux through the reverse shock supports the forward shock an mitigates its deceleration. A rough estimate of the forward shock Lorentz factor as it propagates into the wind can be obtained from equating the energy that crossed the reverse shock with the energy given to the shocked wind<sup>3</sup>,  $m_*(\Gamma_{sh})\Gamma_{sh} \approx m_w \Gamma_{sh}^2$  where  $m_w = 4\pi A R_{sh}$  is the wind mass swept by the shock when its radius is  $R_{sh}$ . Thus, with the equation for  $E_*$  we obtain  $\Gamma_{sh} = \gamma_{*,1}^{0.68} (m_{*,1}/m_w)^{0.32}$ . In order to relate the shock Lorentz factor to the fraction of the shock energy that escapes to the observer, f, we use equation 13, which dictates that once escape starts  $\tilde{\tau}_w(R_{sh}) = \kappa A/R_{sh} = \mu \Gamma_{sh}/f$ . This implies

$$\Gamma_{sh}(f) = \frac{\gamma_{*,1}}{40} \tau_{w,*}^{0.95} f^{-0.48} \approx 1.2 E_{53}^{1.7} M_{ej,5}^{-1.2} R_{*,11}^{-0.95} \tau_{w,*}^{-0.95} f^{-0.48}$$
(20)

and

$$R_{sh}(f) \approx 1.7 \times 10^{14} E_{53}^{-1.7} M_{ej,5}^{1.2} R_{*,11}^{1.95} \tau_{w,*}^{1.95} f^{1.48} \text{ cm}$$
 (21)

where  $\tau_{w,*} = \kappa A/R_*$  is the total optical depth of the wind

from the stellar surface to infinity, which is often of the order of unity in WR stars. As the shock propagates f increases while  $\Gamma_{sh}$  decreases. The breakout takes place either when f approaches unity or when the shock becomes Newtonian and its temperature drops to  $\sim 50-100$  keV, so pair production is not efficient enough and the shock cannot generate its own optical depth anymore.

If  $\Gamma_{sh}(f=1)>1$  then the breakout is relativistic  $(\Gamma_{bo}>1)$  and its properties are obtained by setting f=1 and plugging equations 20 and 21 into equations 15-17. The duration of the breakout emission is then

$$t_{bo} \approx 2000 E_{53}^{-5.1} M_{ei,5}^{3.6} R_{*,11}^{3.85} \tau_{w,*}^{3.86} \text{ s} \qquad (\Gamma_{bo} > 1),$$
 (22)

its temperature at  $t \sim t_{bo}$  is

$$T_{obs,bo} \approx 250 E_{53}^{1.7} M_{ej,5}^{-1.2} R_{*,11}^{-0.95} \tau_{w,*}^{-0.95} \text{ keV} \quad (\Gamma_{bo} > 1), (23)$$

and the total emitted energy is

$$E_{bo} = 10^{48} E_{53}^{1.7} M_{ei.5}^{-1.2} R_{*.11}^{1.05} \tau_{w.*}^{1.05} \kappa_{0.2}^{-1} \text{ erg} \qquad (\Gamma_{bo} > 1).$$
 (24)

The rise time of the breakout emission is much shorter than  $t_{bo}$  and from the evolution of emission with f (equations 15-17 and 20-21) we find that during the pulse the luminosity is almost constant

$$L_{bo} \propto t^{0.03} \qquad (\Gamma_{bo} > 1), \tag{25}$$

and the temperature drops slowly

$$T_{obs} \propto t^{-0.2} \qquad (\Gamma_{bo} > 1). \tag{26}$$

If  $\Gamma_{sh}(f=1) < 1$  then the breakout takes place when the shock becomes mildly relativistic or Newtonian at

$$R_{bo} \approx R_{sh}(\Gamma_{sh} \approx 1) \approx 3 \times 10^{14} E_{53}^{3.57} M_{ej,5}^{-2.52} R_{*,11}^{-1} \tau_{w,*}^{-1} \text{ cm} \quad (\Gamma_{bo} \approx 1),$$
(27)

assuming that  $\tau_w < 1$  at this location. The duration of the breakout emission is then simply

$$t_{bo} \approx \frac{R_{bo}}{c} \approx 10^4 E_{53}^{3.57} M_{ej,5}^{-2.52} R_{*,11}^{-1} \tau_{w,*}^{-1} \text{ s} \qquad (\Gamma_{bo} \approx 1), \quad (28)$$

and the temperature is

$$T_{obs,bo} \approx 50 - 100 \text{ keV} \quad (\Gamma_{bo} \approx 1).$$
 (29)

The total emitted energy is roughly  $4\pi A R_{bo}c^2$ , which depends only on the explosion energy and ejecta mass,

$$E_{bo} \approx 2 \times 10^{48} E_{53}^{3.57} M_{ej,5}^{-2.52} \kappa_{0.2}^{-1} \text{ erg} \quad (\Gamma_{bo} \approx 1).$$
 (30)

while the luminosity depends only on the progenitor radius and wind density

$$L_{bo} \approx 2 \times 10^{44} R_{*,11} \tau_{w,*} \kappa_{0.2}^{-1} \text{ erg/s} \quad (\Gamma_{bo} \approx 1).$$
 (31)

### 5.2.2 Aspherical explosion

The results derived above are for spherical explosions. However, relativistic shock breakouts may also occur when the shock is driven by a relativistic jet, such as in GRBs and conceivably also in some SNe that are not associated with GRBs (e.g., Piran et al. 2017). In long GRBs the jet successfully penetrates through the star and propagates into the circumstellar medium, driving a relativistic shock into that medium. If the jet's opening angle lies within the observer's line-of-sight then the emission from the jet (the GRB prompt emission) is expected to outshine the emission from

 $<sup>^2</sup>$  The notation here is different than in Nakar & Sari (2012). They use the symbols  $m_0$  for the mass that have an optical depth  $\tau=1$  before the explosion and  $\gamma_{f,0}$  for its final Lorentz factor after shock crossing and expansion.

 $<sup>^3</sup>$  Note that the shocked wind material has an internal energy of  $\sim \Gamma m_p c^2$  per baryon and a bulk Lorentz factor  $\sim \Gamma_{sh}$ , hence the energy in the shocked wind is  $\propto m_w \Gamma_{sh}^2$ .

the breakout of that shock. However, a relativistic shock is expected to be driven into the cirum-burst medium also away from the jet opening angle by the cocoon inflated as the jet drives its way through the star (e.g., Ramirez-Ruiz et al. 2002; Lazzati et al. 2010; Nakar & Piran 2017). In the case of long GRBs the properties of the shock driven by the emerging cocoon (its opening angle and Lorentz factor) depend on the mixing between the jet and the stellar material (Nakar & Piran 2017) and therefore can be assessed only using numerical simulations (e.g., ?). We therefore defer the analysis of the shock breakout through a wind in this case for a future work.

There is strong evidence (e.g., Bromberg et al. 2012) that not in all GRBs the relativistic jets are powerfull enough to penetrate through the progenitor. Instead, the jet dies while still inside the star, leaving a collimated hot cocoon. Such events are called choked GRBs. There are also indications that suggest that choked jets may be rather common in some types of core-collapse SNe that are not associated with GRBs (Piran et al. 2017). The cocoon left by a choked jet continues to propagate through the star and emerges into the circumstellar medium. Depending on the energy deposited by the jet, its opening angle and the depth at which the jet is choked, the shock driven by the cocoon can be highly relativistic. in fact as long as the shock Lorentz factor is higher than the inverse of its opening angle, the spherical theory derived above can be applied for observers that have their line-of-sight within the shock opening angle. For these observers the emission can be estimated simply by replacing the total energy in the shock by its isotropic equivalent energy. For example, a typical GRB jet can deposit about  $10^{51} - 10^{52}$  erg within an opening angle of 0.2 rad. If the jet dies after crossing about half of the progenitor's envelope, then the emerging cocoon will drive a shock with an isotropic equivalent energy of  $E_{iso} \sim 5 \times 10^{52}$  -  $5 \times 10^{53}$ erg and an opening angle of about 0.2 rad. The spherical theory is applicable then as a rough approximation for an observer whose line-of-sight falls within this opening angle, by replacing E with  $E_{iso}$ , as long as  $\Gamma_{bo} \gtrsim 5$ .

Finally, we note that an aspherical breakout from a wind is much simpler to model than an oblique shock breakout from a star. In the latter case the acceleration of the shock leads to a steepening of the shock front angle and the breakout dynamics can become highly nontrivial (Matzner et al. 2013; Salbi et al. 2014). In contrast, a shock that propagates in a wind decelerates and finding its Lorentz factor and shape for a given astrophysical setting is straightforward, although in non-spherical configurations numerical simulations are often needed.

## 5.3 The difference between a shock breakout from a wind and from a star

The signature of a relativistic shock breakout from the surface of a star, which was discussed by Nakar & Sari (2012), is different than the signature of a breakout from a stellar wind. There are two major differences between the dynamics of shock propagation near the stellar edge and within a stellar wind that reflect on the observed signature. First, near the stellar edge the shock accelerates, while in the wind it decelerates. Second, near the stellar edge the shock velocity varies significantly (from being Newtonian to relativistic)

within a very narrow range of radii, while in the wind  $\Gamma_{sh}$ varies on the scale of  $R_{sh}$ . As a result, a shock that propagates near a stellar edge deposits decreasing amounts of energy in an increasingly faster material. After shock breakout all the shocked material expands and the energy deposited by the shock during its acceleration is released. The observer then sees emission that originated from material with a range of Lorentz factors, where the total emitted energy is not dominated by the radiation released in the shock breakout itself. Instead it is dominated by the energy deposited in material with an optical depth  $\tilde{\tau} \approx 1$ , namely  $m_{*,1}$ . The closure relation derived by Nakar & Sari (2012) for breakout from a star is for the emission released from  $m_{*,1}$  after it has reached its final Lorentz factor  $\gamma_{*,1}$ . In contrast, in case of a wind the shock decelerates and all the internal energy is accumulated between the reverse and forward shocks, where the material has a roughly uniform Lorentz factor, which is comparable to the shock Lorentz factor. The emission is then dominated, at all times, by the leakage of photons from the shock front, and it peaks when  $f \approx 1$ , at which point the entire energy in the shocked region is released to the observer.

### 6 SUMMARY

In this paper we considered a relativistic shock breakout from a stellar wind, assuming that the evolution of the system is sufficiently slow, so that the structure of the shock can be described, to a good approximation, by a steady solution at the local wind conditions. We further assumed that throughout the shock evolution the immediate downstream temperature is regulated by vigorous pair production, and is maintained at a level of  $\sim 200$  kev. Under these assumptions we constructed an analytic model for a finite RRMS that incorporates photon losses, and employed it to obtain self-consistent shock solutions that are characterized by the fraction of downstream photons that escape to infinity. Our model generalizes the analytic model developed by Nakar & Sari (2012) for infinite, planar RRMS, based on the numerical solutions of Budnik et al. (2010). These RRMS are unique in that they self-generate there own optical depth via pair production and, therefore, can propagate also in a medium at which the total optical thickness ahead of the shock is much smaller then unity. The assumption that the steady solution provides a good description of the shock structure at any given time needs to be verified with detailed, time dependent models, as it is unclear at present whether, and under which conditions, the solution we obtained is stable. We leave this problem for a future work.

Our analysis reveals that once photons start leaking through the upstream of a RRMS, the shock width shrinks by virtue of accelerated pair creation that self-generates the opacity required to sustain the shock radiation mediated. As a result, the breakout from a stellar wind is a gradual process wherein the fraction of the shock energy that leaks to the observer increases continuously over several decades in time and radius. This is in contrast to Newtonian radiation-mediated shocks in which the optical depth is contributed solely by the electrons that incident into the shock from far upstream, in which case the breakout of the shock and its transition to a collisionless shock occurs within about one

dynamical time after photon leakage commences. A complete breakout of a RRMS takes place only when it reaches a radius beyond which the total optical depth of the wind becomes  $\sim \Gamma_{sh}/1000 \ll 1$ . This implies that in an explosion of a typical WR star that is powerful enough to drive a relativistic shock at the stellar edge, shock breakout is expected to occur from the wind at a radius much larger than the stellar radius, since the optical depth of a typical WR wind is of order unity.

By combining our analytic shock solution with existing solutions for the profile of the ejecta emerging at the stellar edge, we were able to predict the observational signature of a RRMS breakout through a wind, which is different than the signature of a breakout from a stellar surface (see section 5.3). First we find the dependence of the duration, temperature and energy of the breakout emission on the breakout radius and Lorentz factor (equations 15-17), and show that these three observables must satisfy a closure relation (equation 18). We then find the signal expected from a spherical explosion of a star. A RRMS in the stellar wind is generated if the explosion is energetic ( $\sim 10^{52} - 10^{53}$  erg), the progenitor is relatively compact ( $\sim 10^{11}$  cm) and the wind optical depth is of order unity. A similar signal may be generated by a non-spherical explosion where a choked jet deposits  $\sim 10^{51} - 10^{52}$  erg within an opening angle of  $\sim 10$  deg (Piran et al. 2017), if the observer's line-of-sigh falls within the jet opening angle. For our canonical parameters, the expected signal is dominated by emission of gamma-rays ( $\sim$ MeV) and its energy is  $\sim 10^{48}$  erg. Its duration, and thus also the luminosity, depends very strongly on the various parameters and can range from a fraction of a second to thousands of seconds. Such a signal may be detectable by gamma-ray observatories like Swift and Fermi out to a distance of  $\sim 10 - 100$  Mpc.

### ACKNOWLEDGEMENTS

We thank Re'em Sari for enlightening discussions. Support by The Israel Science Foundation (grant 1277/13) is acknowledged. AG and EN where partially supported by an ERC starting grant (GRB/SN) and by the I-Core center of excellence of the CHE-ISF.

# APPENDIX A: DERIVATION OF SHOCK EQUATIONS

We consider a planar shock propagating along the positive z-direction at a velocity  $\vec{\beta} = \beta \hat{z}$  (the fluid, in the shock frame, moves in the opposite direction). We treat the plasma inside the shock as a mixed fluid consisting of protons, electrons, positrons and photons in thermal equilibrium. For convenience we distinguish between the electrons advected into the shock by the upstream flow and the pairs produced inside the shock through  $\gamma\gamma$  annihilation. The proper density of the former is denoted by  $n_e$  and of the latter by  $n_{\pm}$ . Charge conservation implies  $n_e = n$  and  $n_- = n_+$ , where n denotes the proper baryon density. Baryon number conservation,

$$\partial_{\mu}(nu^{\mu}) = 0, \tag{A1}$$

here  $u^{\mu} = \Gamma(1, -\beta, 0, 0)$  denotes the bulk 4-velocity of the mixed fluid with respect to the shock frame, implies that  $\Gamma n$  is conserved in the relativistic limit  $\beta \simeq 1$ , and must equal the far upstream value, viz.,  $\Gamma n = \Gamma_u n_u$ . We further denote the proper density of photons streaming with the flow (i.e., moving from the upstream to the downstream) by  $n_{\gamma \to d}$  and the proper density of counterstreaming photons by  $n_{\gamma \to u}$ . The counterstreaming photons are inverse Compton scattered by the inflowing electrons and positrons, and are annihilated via interactions with scattered photons that are moving with the bulk flow. We suppose that the bulk flow and the counter-streaming photons are both highly beamed and adopt the two-beam approximation, that hold in the region where the flow is sufficiently relativistic. The change in the number density of counterstreaming photons is then governed by the equation

$$\frac{dn'_{\gamma \to u}}{dz} = -[\sigma_{KN}(n'_{\pm} + n'_e) + \sigma_{\gamma\gamma}n'_{\gamma \to d}]n'_{\gamma \to u},\tag{A2}$$

where superscript "prime" refers to quantities measured in the shock frame, that is,  $n_e' = \Gamma n_e, n_\pm' = \Gamma n_\pm$ , etc., and  $\sigma_{KN}$ ,  $\sigma_{\gamma\gamma}$  are the full cross-sections for Compton scattering and pair-production, respectively. The change in the density of pairs and downstream moving photons are likewise given by

$$\frac{dn'_{\pm}}{dz} = -2\sigma_{\gamma\gamma}n'_{\gamma\to d}n'_{\gamma\to u},\tag{A3}$$

and

$$\frac{dn'_{\gamma \to d}}{dz} = -[\sigma_{KN}(n'_{\pm} + n'_e) - \sigma_{\gamma\gamma}n'_{\gamma \to d}]n'_{\gamma \to u}.$$
 (A4)

The net density of quanta (pairs + photons) produced inside the shock via conversion of counterstreaming photons is given by  $n_l = n_{\pm} + n_{\gamma \to d}$ . Combining Eqs. (A3) and (A4) yields

$$\frac{dn'_l}{dz} = -[\sigma_{KN}(n'_{\pm} + n'_e) + \sigma_{\gamma\gamma}n'_{\gamma \to d}]n'_{\gamma \to u}.$$
 (A5)

Subtracting equation A5 from equation A2 we readily obtain  $d(n'_{\gamma \to u} - n'_l)/dz = 0$ . Using the far upstream boundary condition  $n'_l(z \to \infty) = 0$  then gives

$$n'_{\gamma \to u} = n'_l + n'_{esc},\tag{A6}$$

where  $n'_{esc} = n'_{\gamma \to u}(z \to \infty)$  denotes the number density of counterstreaming photons that escape the shock to infinity. The last equation simply means that every photon that moves from the immediate downstream towards the upstream either escape the shock or eventually comes back in the form of a scattered photon or a member of an electron-positron pair.

It is convenient to use the net optical depth for conversion of counterstreaming photons

$$d\tau = [\sigma_{KN}(n'_{+} + n'_{e}) + \sigma_{\gamma\gamma}n'_{\gamma \to d}]dz, \tag{A7}$$

and the fractions  $x_l = n_l'/n'$ ,  $x_{esc} = n_{esc}'/n'$ , as free variables. The above rate equations then reduce to the single equation

$$\frac{dx_l}{d\tau} = -(x_l + x_{esc}). \tag{A8}$$

The energy momentum tensor of the mixed fluid is the

sum of the different components,  $T^{\mu\nu}=T^{\mu\nu}_b+T^{\mu\nu}_l+T^{\mu\nu}_{\gamma\to u},$  where

$$T_i^{\mu\nu} = w_i u^{\mu} u^{\nu} + q^{\mu\nu} p_i \tag{A9}$$

for plasma component i ( $i=b,l,\gamma \to u$ ), and  $p_i,w_i$  are the corresponding pressure and specific enthalpy. Since the temperature inside the shock is roughly  $\Gamma m_e c^2$ , the downstream moving leptons are relativistic and we henceforth adopt the approximation  $w_l=4p_l=4n_lkT,w_b=nm_pc^2+4n_ekT$ , neglecting the electron rest mass in the latter expression. The energy of counterstreaming photons, on the other hand, is typically  $m_e c^2$ , so that inside the shock, where  $\Gamma >> 1$ , their contribution to energy and momentum balance can be neglected. Under this approximation the net energy flux can be expressed as,

$$T^{0x} = \Gamma^2 \beta [m_p c^2 n + 4(n_e + n_l) m_e c^2 \hat{T}] = m_p c^2 n \Gamma^2 \beta (1 + (x_l + 1)\mu \hat{T}),$$
(A10)

in terms of the mass ratio  $\mu=m_e/m_p$  and the dimensionless temperature  $\hat{T}=kT/m_ec^2$ . Energy conservation,  $\partial_\mu T^{0\mu}=0$ , the boundary conditions  $x_l(z\to\infty)=\hat{T}(z\to\infty)=0$ ,  $\Gamma(z\to\infty)=\Gamma_u$ , and baryon number conservation,  $n\Gamma\beta=n_u\Gamma_u\beta_u$ , then yield the conservation law:

$$\Gamma(1 + (x_l + 1)\mu\hat{T}) = \Gamma_u. \tag{A11}$$

### REFERENCES

```
Balberg S., Loeb A., 2011, MNRAS, 414, 1715
Barniol Duran R., Nakar E., Piran T., Sari R., 2015, MNRAS,
Bromberg O., Mikolitzky Z., Levinson A., 2011, ApJ, 733, 85
Bromberg O., Nakar E., Piran T., Sari R., 2012, ApJ, 749, 110
Budnik R., Katz B., Sagiv A., Waxman E., 2010, ApJ, 725, 63
Chevalier R. A., Irwin C. M., 2011, ApJ, 729, L6
Johnson M. H., McKee C. F., 1971, Phys. Rev. D, 3, 858
Lazzati D., Morsony B. J., Begelman M. C., 2010, ApJ, 717, 239
Matzner C. D., Levin Y., Ro S., 2013, ApJ, 779, 60
Nakar E., Sari R., 2012, ApJ, 747, 88
Nakar E., 2015, ApJ, 807, 172
Nakar E., Piran T., 2017, ApJ, 834, 28
Ofek E. O., et al., 2010, ApJ, 724, 1396
Pan M., Sari R., 2006, ApJ, 643, 416
Piran T., Nakar E., Mazzali P., Pian E., 2017, preprint,
   (arXiv:1704.08298)
\mbox{Ramirez-Ruiz} \quad \mbox{E.,} \quad \mbox{Celotti} \quad \mbox{A.,} \quad \mbox{Rees} \quad \mbox{M.} \quad \mbox{J.,}
   Mon. Not. R. Astron. Soc. Vol. 337, Issue 4, pp. 1349-1356.,
   337, 1349
Salbi P., Matzner C. D., Ro S., Levin Y., 2014, ApJ, 790, 71
Svirski G., Nakar E., 2014a, ApJ, 788, 113
Svirski G., Nakar E., 2014b, ApJ, 788, L14
Tan J. C., Matzner C. D., McKee C. F., 2001, ApJ, 551, 946
```